Check for updates

High Power Laser Science and Engineering, (2026), Vol. 14, e74, 7 pages.
doi:10.1017/hpl.2026.10166

HIGH POWER LASER SCIENCE AND ENGINEERING

RESEARCH ARTICLE

Evolution of temporal coherent noise in high-peak-power chirped-pulse amplification lasers: experiments and modeling

Xun Chen[1,2,†], Zongxin Zhang[1,†], Xinliang Wang[1], Jiayan Gui[1], Kegui Xia[1], Xiaojun Yang[1], Fenxiang Wu[1], Yi Xu[1], and Yuxin Leng[1]

[1] *State Key Laboratory of Ultra-intense Laser Science and Technology, Shanghai Institute of Optics and Fine Mechanics (SIOM), Chinese Academy of Sciences, Shanghai, China*

[2] *Center of Materials Science and Optoelectronics Engineering, University of Chinese Academy of Sciences, Beijing, China*

(Received 26 January 2026 UTC; revised 28 April 2026 UTC; accepted 28 May 2026 UTC)

Abstract

The optics roughness in Öffner stretchers has been widely identified as a major cause of temporal contrast degradation at tens of picoseconds before the main pulse. However, we find that amplifier-induced noise may become the decisive factor for temporal contrast deterioration at a similar time window with the increase of the B-integral in chirped-pulse amplification systems. Even employing a high-precision convex mirror with root-mean-square roughness values better than 0.2 nm, the experimental measurements show that amplifier-induced noise generates asymmetric profiles under nonlinear effects – exhibiting an obvious pre-pedestal growth proportional to the accumulated B-integral. Analogous to post-to-pre-pulse conversion dynamics, the numerical simulations demonstrate the impact of the B-integral on the pre-pedestal, especially when the pulse peak power scales from the terawatt level to the petawatt level.

Keywords: chirped-pulse amplification; coherent pedestal; temporal contrast; ultra-high-intensity lasers

1. Introduction

With the great advances in chirped-pulse amplification (CPA)[1], the development of high-intensity femtosecond laser systems has been dramatically accelerated. The peak power of femtosecond lasers has advanced from the terawatt (TW)[2] to the petawatt (PW)[3–5] level, and high focused intensities of 10^{22} W/cm^2 or more have become available at laboratories around the world. Under such extreme intensities, the temporal contrast ratio (TCR) emerges as a critical parameter, as dictated by strong-field physics requirements. When pre-pulses or pedestal noises exceed 10^{-12} relative to the peak intensity, these temporal noises can interact with the target material prematurely (on ps-to-ns timescales), inducing significant pre-ionization. This alters the initial target conditions (e.g., density, ionization degree), thereby perturbing the ultrafast dynamics between the main pulse and the target.

Temporal contrast degradation arises from three dominant noise sources: the amplified spontaneous emission (ASE), pre-pulse and coherent pedestals. Over the past decade, significant progress in temporal contrast enhancement techniques – including double-chirped-pulse amplification (double-CPA)[6], saturable absorbers (SAs)[7,8], optical parametric amplification (OPA)[9,10] and cross-polarized wave generation (XPWG)[11–13] – has enabled effective suppression of ASE in femtosecond lasers. Pre-pulses can be categorized into linear-origin pre-pulses and those converted via nonlinear effects. The former primarily originate from multiple reflections in optical components[14] or scattering noise induced by diffraction gratings in the stretcher[15,16]. The latter are mainly generated by post-pulses from the multiple reflection in optical components, due to the nonlinear coupling associated with the B-integral accumulation in CPA[17] or the instantaneous gain effect in OPA[18,19]. The origin mechanisms of such pre-pulses have been extensively investigated through both theoretical and experimental studies[20–22]. In addition, these studies demonstrate that optimizing the laser optical path configuration[14,23]

Correspondence to: Y. Xu and Y. Leng, State Key Laboratory of Ultra-intense Laser Science and Technology, Shanghai Institute of Optics and Fine Mechanics (SIOM), Chinese Academy of Sciences, Shanghai 201800, China. Emails: xuyi@siom.ac.cn (Y. Xu); lengyuxin@mail.siom.ac.cn (Y. Leng)

[†]These authors contributed equally to this work.

© The Author(s), 2026. Published by Cambridge University Press in association with Chinese Laser Press. This is an Open Access article, distributed under the terms of the Creative Commons Attribution licence (https://creativecommons.org/licenses/by/4.0), which permits unrestricted re-use, distribution and reproduction, provided the original article is properly cited.

https://doi.org/10.1017/hpl.2026.10166 Published online by Cambridge University Press

or employing wedge-angle optical elements[15,24] can effectively eliminate pre- and post-pulses.

Coherent pedestals appearing within hundreds of picoseconds of the main pulse are attributed to two dominant mechanisms: surface roughness in the stretcher optics induces random spatio-phase noise (RSPN), degrading the temporal coherence of the main pulse and generating a noisy temporal pedestal (stretcher-generated coherent noise); the formation of the post-pedestal during pulse amplification introduces structural asymmetry in the coherent pedestal profile. Subsequent nonlinear processes drive the conversion of this post-pedestal into a pre-pedestal as amplification proceeds (amplifier-induced coherent noise). For the former case, computational modeling and experiments[25] confirm that the surface quality of the convex mirror in Öffner stretchers directly degrades the TCR. Recent experimental studies[26] have quantitatively characterized the impact of RSPN on pulse contrast, demonstrating a strong correlation between the temporal pedestal and the roughness of the convex mirror in Öffner stretchers. Experimental measurements performed on the J-KAREN-P laser system[23] further confirm that replacing the conventional mirror (root-mean-square (RMS) roughness: ~10 nm) with a high-quality convex mirror (RMS roughness: 0.2–0.3 nm) leads to significant suppression of coherent noise in the pulse temporal profile. Regarding the latter, systematic studies reveal that the post-pedestal induces structural asymmetry in the coherent pedestal profile, arising from the gain medium in CPA systems. Furthermore, the post-pedestal-to-pre-pedestal conversion efficiency exhibits a clear scaling dependence on the accumulated B-integral[27]. Furthermore, numerical and experimental investigations also reveal post-pedestal-to-pre-pedestal conversion dynamics in optical parametric chirped-pulse amplification (OPCPA) systems[28]. While both generation mechanisms have been well-studied individually, their relative contributions to the final pedestal after high-power amplification in CPA systems remain debated. Here, we investigate the distinct evolution characteristics of these two dominant coherent noise sources (stretcher-generated and amplifier-induced) during high-power amplification and quantify their relative impacts on the temporal contrast of output pulses.

This study provides systematic experimental and numerical evidence revealing distinct evolutionary characteristics between stretcher-generated and amplifier-induced pedestals in high-power amplification. Crucially, we demonstrate their independent development dynamics through practical laser-system contrast degradation analysis, and further identify the pre-pedestal – resulting from post-pedestal conversion in high-power CPA – as the primary determinant of ultrashort pulse TCR degradation. The study is organized as follows. Firstly, we present the home-made 200-TW CPA system and experimentally measure the TCR of pulses at different amplification conditions after adopting an ultra-low-roughness convex mirror (RMS <0.2 nm), revealing the anomalous growth of asymmetric coherent noise (Section 2). Secondly, our numerical model systematically analyzes the distinct evolution mechanisms of both critical coherent noise sources (Section 3). Thirdly, using our numerical model, we investigate the evolution of pre-pedestal structures under higher B-integral conditions relevant to PW-class laser systems (Section 4). Finally, by analyzing experimental data and simulation results, we identify that the nonlinear effect of trailing-to-leading-edge coherent noise conversion during high-power amplification in the CPA system plays a decisive role in limiting the ultimate TCR of ultrashort laser pulses.

2. System performance and noise dynamics in a 200-TW chirped-pulse amplification laser

The home-made Ti:sapphire (Ti:sa) laser at the Shanghai Institute of Optics and Fine Mechanics (SIOM) facility was constructed in 2015 and has been further upgraded to improve the pulse contrast[2,29]. A simplified layout of the 200 TW/1 Hz Ti:sa laser is shown in Figure 1. The first CPA stage (Coherent, Astrella) provides a 40 fs seed pulse with energy of 6 mJ at a 1 kHz repetition rate, which is transmitted through a compact nonlinear temporal filter. The nonlinear temporal filter combining XPWG and fs-OPA can deliver cleaned pulses at a 1 kHz repetition rate with energy of 100 μJ and the TCR of the seed pulse can be optimized up to 10^{-11} with a significantly suppressed pedestal, as shown in Figure 2[11,12]. The trailing- and leading-edge coherent noises exhibit comparable magnitudes. The picosecond temporal contrast measurement was performed using a scanning third-order cross-correlator (TOCC; Sequoia, Amplitude Laser), which provides an intrinsic dynamic range of up to 11 orders of magnitude.

The seed pulse is then re-stretched using a grating-based all-reflective Öffner stretcher for the second CPA stage, and an acousto-optic programmable dispersive filter (AOPDF; Dazzler, Fastlite) is implemented to compensate for high-order dispersion terms resulting from beam propagation. Before entering the regenerative amplifier, a single pulse at a 10 Hz repetition rate is selected by a Pockels cell (PC) assembly that consists of two high extinction ratio Glan laser polarizers and a KD*P PC. The 10 Hz laser pulse is amplified to 1.5 mJ in the regenerative amplifier with pump energy of 35 mJ. After passing through another two PC assemblies, the repetition rate of the laser pulse is changed from 10 to 1 Hz. Subsequently, the pulse is amplified to 8 J through a multi-pass pre-amplifier (MPA-1), a power amplifier (MPA-2) and a final amplifier (MPA-3). The amplified laser pulse is delivered into a vacuum compressor, and the pulse duration of 27 fs is achieved.

To ensure a consistent dynamic range in our measurements while characterizing coherent noise evolution throughout the

https://doi.org/10.1017/hpl.2026.10166 Published online by Cambridge University Press

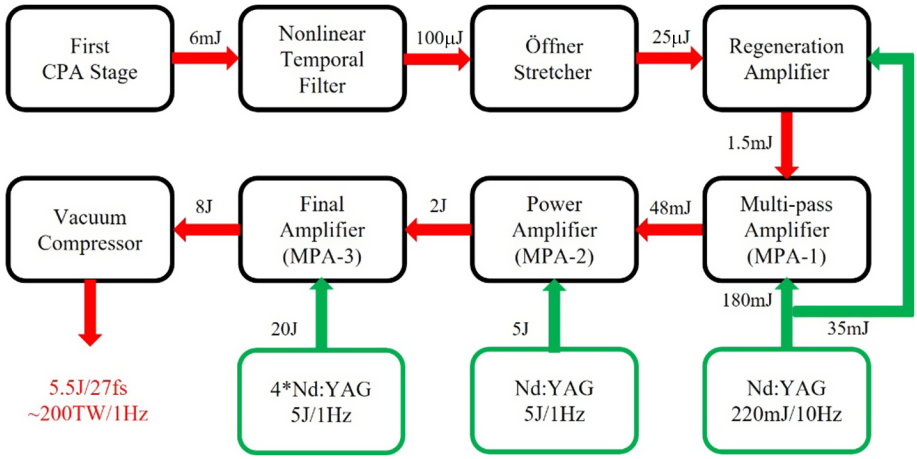


Figure 1. Layout of the 200 TW/1 Hz Ti:sapphire laser system.

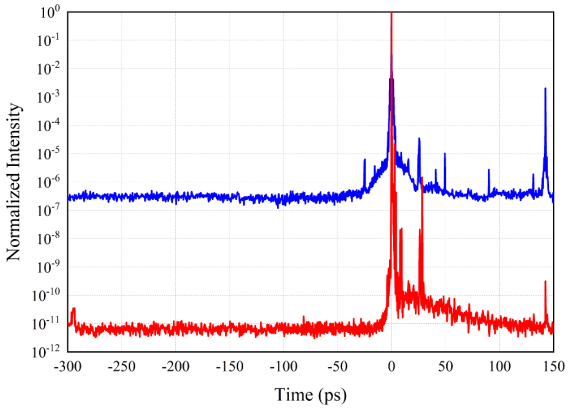


Figure 2. Measured temporal contrast before (blue line) and after (red line) the nonlinear temporal filter.

amplification stages, we conducted comparative TCR analysis using a TOCC under two amplification conditions: low-energy amplification (only the regenerative amplifier and MPA-1 work) and high-energy amplification (all amplifiers work). For both amplification conditions, the chirped pulses traveled through nearly identical optical paths in the laser system. The resulting compressed femtosecond pulses were sampled by a pick-off mirror inside the compressor and subsequently directed into the TOCC for TCR characterization. Active spectral control via the AOPDF ensured a consistent output spectral width and profile under the different amplification conditions. Furthermore, to maintain constant energy levels at the TOCC under the different amplification conditions, an adjustable attenuator – consisting of uncoated wedges and pick-off mirrors with different splitting ratios – was implemented in the measurement beam path.

According to the experimental results reported in Ref. [23], integrating optical components with superior surface roughness in the laser system, we can effectively suppress stretcher-generated coherent noise. This approach enables clearer observation of amplifier-induced noise evolution and facilitates investigation into potential interactions between the two noise sources. In this work, we replaced the original convex mirror (RMS roughness: 1–2 nm) with newly fabricated high-precision optics with less than 0.2 nm RMS roughness. The surface roughness measured by the ZYGO laser interferometer is shown in Figure 3. The old convex mirror (Figure 3(a)) exhibits an RMS roughness of approximately 1.18 nm, whereas the new convex mirror (Figure 3(b)) yields an RMS value of approximately 0.14 nm. The reduction in surface roughness effectively suppresses stretcher-generated noise, thereby enabling more precise observation and comparative analysis of contrast degradation attributable to amplification dynamics.

After replacing the convex mirror, we measured the temporal contrast and optical spectrum (Figure 4) under two amplification conditions: low-energy (27 mJ) and high-energy (5.2 J) operation, as illustrated in Figure 4. The output pulses from both amplification conditions undergo identical compression, yielding a measured pulse width of approximately 27 fs (Fastlite Wizzler). The red and blue curves correspond to the temporal contrast and spectral profiles for the low- and high-energy cases, respectively. The comparison reveals that under high-energy amplification conditions, the pre-pedestal emerges earlier (from −130 ps) and within the leading-edge temporal window (−80 to −10 ps) the coherent noise intensity exhibits a pronounced amplification of approximately one to two orders of magnitude, while the trailing-edge noise retains nearly invariant intensity and structure. Intriguingly, optimizing the stretcher's optical surface quality yields negligible suppression of coherent noise in high-energy amplification regimes. Instead, experimental measurements reveal significant enhancement of the pre-pedestal. Consequently, our experiments reveal the amplification characteristics of the pre-pedestal in high-power CPA systems, although its underlying physical mechanisms and temporal dynamics remain unclear.

https://doi.org/10.1017/hpl.2026.10166 Published online by Cambridge University Press

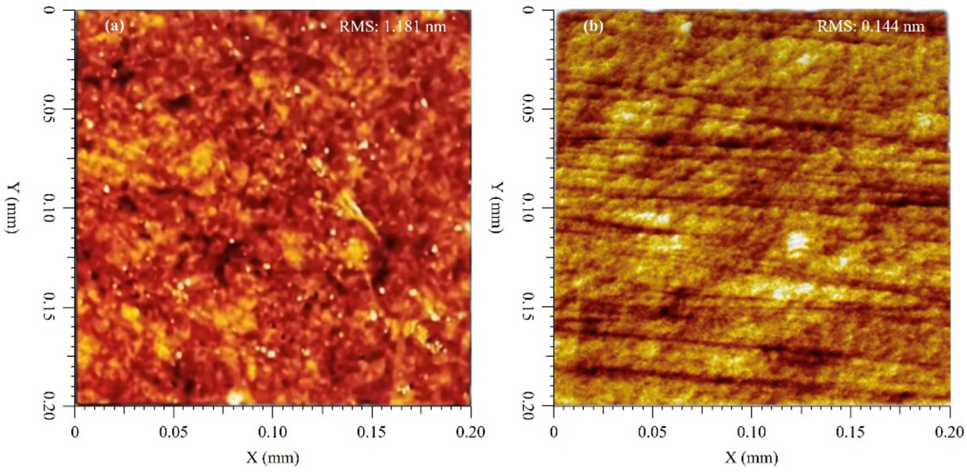


Figure 3. Surface roughness of the convex mirrors measured using laser interferometry.

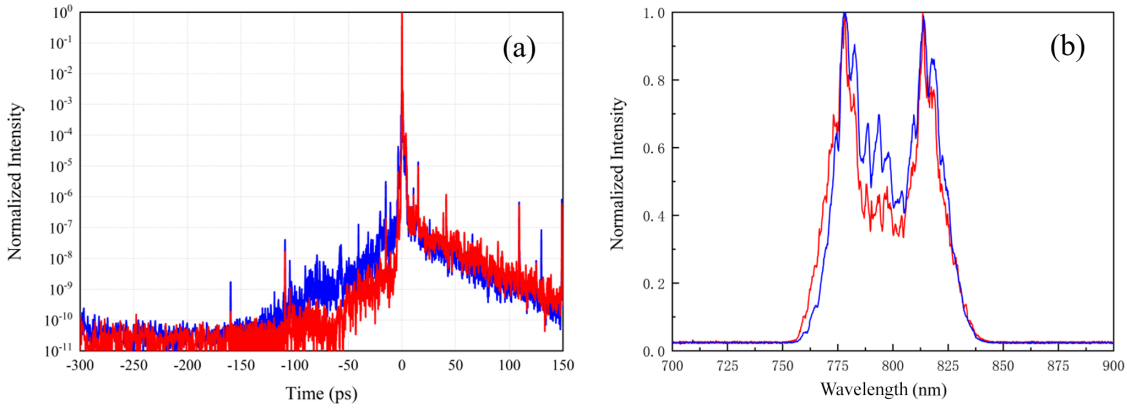


Figure 4. Measured temporal contrast (a) and spectrum (b) under two amplification conditions.

3. Numerical modeling of temporal coherent noise evolution in chirped-pulse amplification systems

Using the established CPA model[20,21], we systematically simulate and analyze the dynamic evolution of two dominant coherent noise sources during high-power amplification. Given the high temporal contrast provided by our nonlinear temporal filter – particularly in suppressing pre-/post-pedestal noise within the coherent noise region (covering 100 ps around the main pulse) – the purified temporal contrast (red line in Figure 2) clearly demonstrates complete suppression of CPA-1-stage coherent noise. Thus, the seed light in simulations is modeled as an ideal super-Gaussian pulse (spectrum with a 10th-order super-Gaussian profile, 50-nm full width at half maximum (FWHM) bandwidth centered at 800 nm). Firstly, we investigate the coherent noise introduced by surface roughness of near-/far-field optics in the stretcher. Building on the universal theoretical and experimental framework established in Ref. [25], we adopt a similar noise modeling approach, in which the spectrum $E(\omega)$ of the optical pulse is analytically expressed as follows:

$$\tilde{E}(\omega) = \sqrt{\tilde{I}(\omega)}\exp[i\varphi(\omega)], \tag{1}$$

where $I(\omega)$ and $\varphi(\omega)$ are the spectral intensity and phase of the field, respectively.

The spectral phase of the pulse is decomposed as $\varphi(\omega) = \varphi_0(\omega) + \delta\varphi(\omega)$, where $\varphi_0(\omega)$ represents a slowly varying spectral phase (e.g., linear or nonlinear chirp) and $\delta\varphi(\omega)$ represents a high-frequency spectral phase modulation of small amplitude. Assuming that the amplitude of $\delta\varphi(\omega)$ is small relative to unity, one can write $\exp[i\delta\varphi(\omega)] \approx 1 + i\delta\varphi(\omega)$. Equation (1) can be rewritten as follows:

$$\begin{aligned}\tilde{E}(\omega) &= \sqrt{\tilde{I}(\omega)}\exp[i\varphi_0(\omega)]\exp[i\delta\varphi(\omega)] \\ &\approx \tilde{E}_0(\omega)[1 + i\delta\varphi(\omega)].\end{aligned} \tag{2}$$

We first investigate the coherent noise evolution induced solely by the stretcher-generated pedestal during high-power amplification. As demonstrated in Ref. [25], the

https://doi.org/10.1017/hpl.2026.10166 Published online by Cambridge University Press

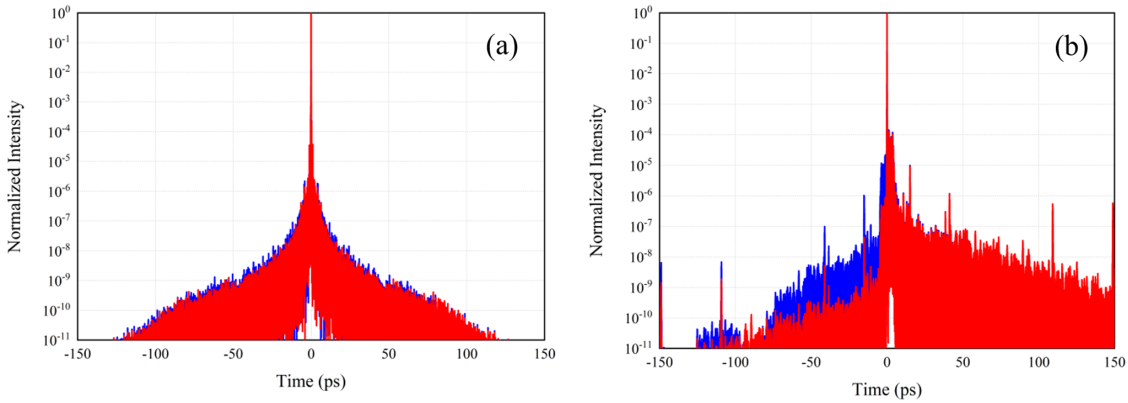


Figure 5. Simulation results of pedestal (stretcher-generated (a) and amplifier-induced (b)) evolution in high-power amplification.

temporal pedestal produced via high-frequency phase modulation in the stretcher exhibits inherent symmetry. To ensure direct comparison with experimental results while eliminating post-pedestal effects from amplifiers, the numerical model employs a stretcher-generated pedestal whose leading-edge pre-pedestal matches the experimentally measured pre-pedestal (red curve) in Figure 4(a), while maintaining a symmetric post-pedestal profile. The pulse function, including coherent noise contributions from optical surface roughness in the stretcher, was then used in simulations to study two different amplification conditions, corresponding to the experimental cases. The simulation results are shown in Figure 5(a), where the red curve represents the simulated temporal contrast of the compressed pulse under the low-energy amplification case, with a total accumulated B-integral of approximately 0.04 rad during propagation in the crystal. The blue curve corresponds to the high-energy amplification case, exhibiting a higher accumulated nonlinear phase (~0.47 rad). Comparative analysis shows that, during high-power amplification in the CPA system, the coherent noise induced by optical surface roughness does not exhibit significant asymmetric distortion. Moreover, the pedestal of this symmetric structure shows no notable intensity enhancement.

Next, we investigate the nonlinear conversion (via self-phase modulation, SPM) of an asymmetric post-pedestal into a pre-pedestal and its evolution during high-power amplification in CPA systems. Following the post-pedestal modeling approach described in Ref. [28], we synthesize an asymmetric post-pedestal consisting of 200 replicas of the main pulse. Each replica is temporally displaced with a random delay, assigned a random phase (0–2π), and scaled in amplitude according to the post-pedestal experimental data corresponding to the red curve in Figure 4(a). The seed pulse embedded with an asymmetric coherent noise structure is propagated through our amplification model, with simulations conducted under both experimental amplification conditions (matching the parameters in Figure 4). The simulation results are shown in Figure 5(b), where the red and blue curves represent the temporal contrast of the compressed pulse under the low-energy and high-energy amplification case, with accumulated B-integrals of approximately 0.04 rad and approximately 0.47 rad during laser propagation, respectively. Notably, the simulated coherent noise exhibits an evolution trend (with a 1–2 orders-of-magnitude growth of pre-pedestal within the leading 100-ps range) closely matching our experimental measurements during high-power CPA.

A detailed comparison between simulations and experimental measurements shows that the simulated pre-pedestal in the range of −75 ps to 0 ps is within 0.5 orders of magnitude lower than the experimentally observed. Given that the numerical model does not account for transmission elements (e.g., beam expanders and electro-optic crystals) in the actual system, we consider this difference to be justified. Furthermore, when simulating the combined effect of both dominant noise sources, the calculated noise intensity and temporal distribution at high-energy amplification condition exhibit negligible deviation from the case where only the latter source is considered, suggesting no significant interaction between the two noise mechanisms. This also explains why replacing with convex mirrors of high-precision surface roughness failed to achieve noticeable TCR improvement under high-energy amplification condition. A qualitative physical explanation aligns with the observed phenomenon. The stretcher-generated pedestal originates from high-frequency spectral phase modulation within the main pulse's spectral bandwidth, primarily caused by surface roughness of far-field optical elements in the stretcher. After stretching, such high-frequency spectral phase modulation converts into temporal intensity modulation through the time-frequency coupling of the chirped pulse. However, its modulation amplitude remains negligible and cannot be effectively amplified by the accumulated B-integral in the laser system. Conversely, the main pulse can temporally overlap with the post-pulses forming the post-pedestal, directly inducing intensity modulation. This intensity modulation is sufficiently strong to be converted into spectral phase modulation via SPM during amplification. Ultimately, the effect replicates from the trailing to leading edge, resulting in significant pre-pedestal growth.

https://doi.org/10.1017/hpl.2026.10166 Published online by Cambridge University Press

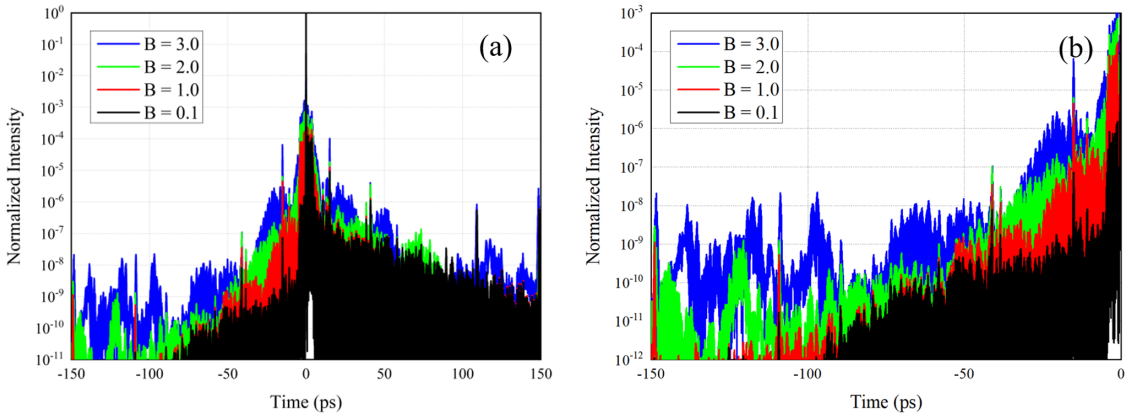


Figure 6. Simulated evolution of coherent noise with increasing B-integral values in TW-to-PW-class laser systems.

4. B-integral dependent coherent noise dynamics during TW-to-PW power scaling

When scaling the output power of CPA laser systems from TW to PW class, the accumulated B-integral during amplification and propagation increases significantly. This enhanced B-integral necessitates careful consideration of the subsequent evolution characteristics of the leading-edge coherent noise. Building upon the established numerical model, we further simulation the nonlinear dynamics in high-power CPA laser systems. Figure 6 systematically investigates the evolution of coherent noise with increasing B-integral accumulation. The simulations retained the same initial laser parameters as the previously modeled 200 TW system. Based on our home-made SULF-10 PW facility[3], the accumulated B-integral in the amplifier system was approximately 1 rad at the 1 PW peak power level, increasing to approximately 2 rad at 10 PW. Under the same amplifier design, further scaling the peak power beyond 10 PW would drive the B-integral to 3 rad or higher. Figure 6(a) quantifies the degradation of temporal contrast as the B-integral rises from 0.1 rad to 3.0 rad, while Figure 6(b) emphasizes the dynamic structural variations of pre-pedestal noise within a 150-ps temporal window preceding the main pulse.

Comparative analysis reveals that as the accumulated B-integral increases during CPA and propagation, the pre-pedestal converted from the trailing-edge coherent noise exhibits growing intensity, demonstrating a strong positive correlation with the B-integral magnitude. Further analysis demonstrates inhomogeneous structural evolution of pre-pedestal. When B-integral $<$ 1 rad, the strongest amplification occurs within the -50 ps to 0 ps temporal window, while no significant enhancement is observed beyond this interval. When B-integral $>$ 1 rad, the growth rate of pre-pedestal within the -50 ps to 0 ps range decelerates, whereas a pronounced enhancement emerges in the region beyond -50 ps (temporally isolated from the main pulse). Concurrently, the trailing-edge coherent noise no longer remains constant but exhibits synchronized degradation with the pre-pedestal. The inhomogeneous structural growth of the pre-pedestal may be qualitatively explained by a mechanism analogous to pre-pulse generation from post-pulses in chirped-pulse amplifiers[20,22]. Similar to post-pulse interactions with the main pulse, the post-pedestal temporally overlaps with the main pulse during high-power amplification, resulting in mutual intensity modulation. Through the self-phase modulation (SPM) effect in CPA systems, this intensity modulation is converted into a nonlinear phase. After compression, these nonlinear phase shifts manifest temporally as a pre-pedestal whose intensity correlates directly with the B-integral value.

Our findings demonstrate that the accumulated B-integral nonlinear phase in CPA laser systems significantly influences the evolution dynamics of coherent noise. When the B-integral exceeds 1 rad, the nonlinear effects induce not only strong amplification of the pre-pedestal but also energy coupling toward the trailing edge. These processes degrade the temporal contrast by two to three orders of magnitude, thereby fundamentally limiting the performance enhancement achievable through higher peak power in ultra-intense ultrafast laser systems.

5. Conclusion

Experimental and numerical studies demonstrate the distinct evolution dynamics of ps-scale coherent noise in high-power CPA laser systems, governed by its origin: stretcher-generated noise maintains symmetric pedestals with negligible distortion during energetic amplification; in contrast, amplifier-induced noise develops asymmetric pedestals, exhibiting pre-pedestal growth proportional to the accumulated B-integral. Through combined simulations and experiments, we confirm that these two coherent noises independently affect the final temporal contrast of the output pulses. Even with stretcher-generated coherent noise suppressed via sub-nanometer optics polishing, its mitigation proves ineffective under high B-integral conditions, where amplifier-induced noise dominates, and

https://doi.org/10.1017/hpl.2026.10166 Published online by Cambridge University Press

ultimately limits the TCR. This effect becomes critical toward the 10 and 100 PW regimes, where contrast control is essential not only for peak intensity but also for enabling next-generation strong-field physics experiments.

Our findings establish the B-integral as a decisive metric for contrast optimization in PW-class CPA lasers, shifting the optimization focus from stretcher design to active management of nonlinear phase accumulation. These results provide guidelines for coherent noise characterization and mitigation, advancing the development of ultra-high-intensity CPA lasers.

Acknowledgements

This work was supported by the National Key R&D Program of China (Grant No. 2025YFF0515102), the Strategic Priority Research Program of Chinese Academy of Sciences (Grant No. XDB0890100), the National Natural Science Foundation of China (Grant No. 12388102) and the Top-notch Project of Shanghai Oriental Talents Program (Comprehensive Platform).

References

1. M. D. Strickland and G. Mourou, Opt. Commun. **55**, 219 (1985).
2. Y. Xu, J. Lu, W. Li, F. Wu, Y. Li, C. Wang, Z. Li, X. Lu, Y. Liu, Y. Leng, R. Li, and Z. Xu, Opt. Laser Tech. **79**, 141 (2016).
3. W. Li, Z. Gan, L. Yu, C. Wang, Y. Liu, Z. Guo, L. Xu, M. Xu, Y. Hang, Y. Xu, J. Wang, P. Huang, H. Cao, B. Yao, X. Zhang, L. Chen, Y. Tang, S. Li, X. Liu, S. Li, M. He, D. Yin, X. Liang, Y. Leng, R. Li, and Z. Xu, Opt. Lett. **43**, 5681 (2018).
4. F. Lureau, G. Matras, O. Chalus, C. Derycke, T. Morbieu, C. Radier, O. Casagrande, S. Laux, S. Ricaud, G. Rey, A. Pellegrina, C. Richard, L. Boudjemaa, C. Simon-Boisson, A. Baleanu, R. Banici, A. Gradinariu, C. Caldararu, B. D. Boisdeffre, P. Ghenuche, A. Naziru, G. Kolliopoulos, L. Neagu, R. Dabu, I. Dancus, and D. Ursescu, High Power Laser Sci. Eng. **8**, e43 (2020).
5. Z. Zhang, F. Wu, J. Hu, X. Yang, J. Gui, X. Liu, C. Wang, Y. Liu, X. Lu, Y. Xu, Y. Leng, R. Li, and Z. Xu, High Power Laser Sci. Eng. **8**, e4 (2020).
6. M. Kalashnikov, E. Risse, H. Schonnagel, and W. Sandner, Opt. Lett. **30**, 923 (2005).
7. H. Kiriyama, A. S. Pirozhkov, M. Nishiuchi, Y. Fukuda, K. Ogura, A. Sagisaka, Y. Miyasaka, M. Mori, H. Sakaki, N. P. Dover, K. Kondo, J. K. Koga, T. Z. Esirkepov, M. Kando, and K. Kondo, Opt. Lett. **43**, 2595 (2018).
8. S. Fourmaux, S. Payeur, S. Buffechoux, P. Lassonde, C. S. Pierre, F. Martin, and J. C. Kieffer, Opt. Express **19**, 8486 (2011).
9. C. Dorrer, I. A. Begishev, A. V. Okishev, and J. D. Zuegel, Opt. Lett. **32**, 2143 (2007).
10. C. Liu, Z. Wang, W. Li, Q. Zhang, H. Han, H. Teng, and Z. Wei, Opt. Lett. **35**, 3096 (2010).
11. L. Yu, Y. Xu, Y. Liu, Y. Li, S. Li, Z. Liu, W. Li, F. Wu, X. Yang, Y. Yang, C. Wang, X. Lu, Y. Leng, R. Li, and Z. Xu, Opt. Express **26**, 2625 (2018).
12. J. Hu, X. Wang, X. Yang, P. Bai, F. Wu, Z. Zhang, H. Chen, X. Yang, J. Qian, J. Gui, Y. Li, Y. Liu, X. Lu, Y. Xu, and Y. Leng, Opt. Express **29**, 37443 (2021).
13. A. Jullien, O. Albert, F. Burgy, G. Hamoniaux, J. P. Rousseau, J. P. Chambaret, F. A. Rochereau, G. Chériaux, J. Etchepare, N. Minkovski, and S. M. Saltiel, Opt. Lett. **30**, 920 (2005).
14. P. Bai, Z. Zhang, X. Wang, F. Wu, J. Hu, X. Yang, J. Qian, J. Gui, X. Lu, Y. Liu, Y. Xu, X. Liang, Y. Leng, and R. Li, Appl. Opt. **61**, 4627 (2022).
15. X. Wang, X. Liu, X. Lu, J. Chen, Y. Long, W. Li, H. Chen, X. Chen, P. Bai, Y. Li, Y. Peng, Y. Liu, F. Wu, C. Wang, Z. Li, Y. Xu, X. Liang, Y. Leng, and R. Li, Ultrafast Sci. **2022**, 9894358 (2022).
16. C. Hooker, Y. Tang, O. Chekhlov, J. Collier, E. Divall, K. Ertel, S. Hawkes, B. Parry, and P. P. Rajeev, Opt. Express **19**, 2193 (2011).
17. N. V. Didenko, A. V. Konyashchenko, A. P. Lutsenko, and S. Y. Tenyakov, Opt. Express **16**, 3178 (2008).
18. J. Wang, P. Yuan, J. Ma, Y. Wang, G. Xie, and L. Qian, Opt. Express **21**, 15580 (2013).
19. X. Wang, X. Lu, X. Guo, R. Xu, and Y. Leng, Chin. Opt. Lett. **16**, 053201 (2018).
20. X. Chen, X. Wang, H. Chen, X. Yang, J. Hu, P. Bai, Y. Zhao, S. Pan, F. Wu, Z. Zhang, Y. Xu, and Y. Leng, Appl. Opt. **62**, 7791 (2023).
21. H. Chen, X. Wang, X. Liu, X. Chen, P. Bai, S. Pan, L. Hu, J. Hu, F. Wu, Z. Zhang, Y. Liu, Y. Xu, and Y. Leng, Opt. Express **31**, 40285 (2023).
22. H. Kiriyama, Y. Miyasaka, A. Sagisaka, K. Ogura, M. Nishiuchi, A. S. Pirozhkov, Y. Fukuda, M. Kando, and K. Kondo, Opt. Lett. **45**, 1100 (2020).
23. H. Kiriyama, Y. Miyasaka, A. Kon, M. Nishiuchi, A. Sagisaka, H. Sasao, A. S. Pirozhkov, Y. Fukuda, K. Ogura, K. Kondo, N. Nakanii, Y. Mashiba, N. P. Dover, C. Liu, M. Kando, S. Bock, T. Ziegler, T. Püschel, H.-P. Schlenvoigt, K. Zeil, and U. Schramm, Photonics **10**, 997 (2023).
24. H. Kiriyama, Y. Miyasaka, A. Kon, M. Nishiuchi, A. Sagisaka, H. Sasao, A. S. Pirozhkov, Y. Fukuda, K. Ogura, K. Kondo, N. P. Dover, and M. Kando, High Power Laser Sci. Eng. **9**, e62 (2021).
25. C. Dorrer and J. Bromage, Opt. Express **16**, 3058 (2008).
26. L. Ranc, C. Le Blanc, N. Lebas, L. Martin, J.-P. Zou, F. Mathieu, C. Radier, S. Ricaud, F. Druon, and D. Papadopoulos, Opt. Lett. **45**, 4599 (2020).
27. N. Khodakovskiy, M. Kalashnikov, E. Gontier, F. Falcoz, and P.-M. Paul, Opt. Lett. **41**, 4441 (2016).
28. B. Webb, C. Feng, C. Dorrer, C. Jeon, R. G. Roides, S. Bucht, and J. Bromage, Opt. Express **32**, 12276 (2024).
29. F. Wu, Z. Zhang, X. Yang, J. Hu, P. Ji, J. Gui, C. Wang, J. Chen, Y. Peng, X. Liu, Y. Liu, X. Lu, Y. Xu, Y. Leng, R. Li, and Z. Xu, Opt. Laser Technol. **131**, 106453 (2020).

https://doi.org/10.1017/hpl.2026.10166 Published online by Cambridge University Press